Original article

Post-mortem computed tomography (PMCT) radiological findings and assessment in advanced decomposed bodies

Compliance with Ethical Standards

Ethical approval: This article does not contain any studies with human participants or animals performed by any of the authors

Original article

Post-mortem computed tomography (PMCT) radiological findings and assessment in advanced decomposed bodies

Authors

Gaia Cartocci[1], Alessandro Santurro[1], Margherita Neri[2], Fulvio Zaccagna[3], Carlo Catalano[4], Raffaele La Russa[1,5], Emanuela Turillazzi[6], Valeria Panebianco[4], Paola Frati[1,5], Vittorio Fineschi[1,5*]

[1] Department of Anatomical, Histological, Forensic and Orthopaedic Sciences, Sapienza University of Rome, Viale Regina Elena 336, 00161 Rome (RM), Italy;

[2] Department of Morphology, Experimental Medicine and Surgery, University of Ferrara, Via Fossato di Mortara 70, 44121 Ferrara (FE), Italy;

[3] Department of Radiology, School of Clinical Medicine, University of Cambridge, Hills Rd, Cambridge CB2 0SP, UK;

[4] Department of Radiological Sciences, Oncology and Anatomical Pathology, Sapienza University of Rome, Viale del Policlinico 155, 00161 Rome (RM), Italy;

[5] IRCSS Neuromed Mediterranean Neurological Institute, Via Atinense 18, 86077 Pozzilli (IS) Italy;

[6] Institute of Legal Medicine, Department of Surgical Pathology, Medical, Molecular and Critical Area, University of Pisa, Via Roma 55, 56126 Pisa (PI), Italy.

*** Corresponding author:** Vittorio Fineschi - Department of Anatomical, Histological, Forensic and Orthopaedic Sciences, Sapienza University of Rome, Viale Regina Elena 336, 00161 Rome, Italy. E-mail: vfinesc@tin.it; Tel: + 39 06 49912722; Fax: + 39 06 49912723

Abstract

Purpose - The aim of the study is to report radiological findings and features in advanced decomposed bodies obtained by post-mortem computed tomography (PMCT) with autopsy correlation.

Materials and methods - This retrospective descriptive multicentric study included 41 forensic cases examined between May 2013 and November 2016. All the bodies were PMCT-scanned prior to autopsy and internal putrefactive state was determined using the radiological alteration index (RAI) by a radiologist with expertise in forensic radiology and a forensic pathologist trained in forensic imaging. After PMCT-scans, grade of external putrefaction (GEP) was assigned during the external examination and the complete autopsy was performed by forensic pathologists.

Results - The PMCT-images evaluation revealed that the RAI index was > 61 in all bodies, corresponding to a moderate-massive presence of putrefactive gas. The gas grade was > II in correspondence of the major vessels, heart cavities, liver parenchyma, vertebra L3 and subcutaneous pectoral tissues, and varied from I to III in correspondence of the kidney. Cadaveric external examination revealed the presence of advanced transformative phenomena, with a GEP3 and GEP4 in most of the cases, with body swelling, eyes and tongue protrusion, body fluids expulsion and fat liquefaction.

Conclusion - Radiological imaging by PMCT as an adjunct to autopsy in advanced decomposed bodies represents a useful tool in detecting post-mortem gas, even in very small amounts. A correct interpretation process of the PMCT-data is essential to avoid images pitfalls, due to natural decomposition that can be mistaken for pathologic processes.

Key words: forensic radiology, post-mortem computed tomography, radiological alteration index, decomposition processes, gas

Introduction

Post-mortem computed tomography (PMCT) was introduced in the late 1970's to describe radiographic patterns of gunshot injuries to the head [1]. Following the most recent advances, CT technology is today frequently requested as a complement before conventional autopsy, or in some cases as a supplement, for non-invasive post-mortem diagnosis [2]. PMCT offers a detailed visualization of anatomical structures, injury patterns or localization of foreign bodies prior to dissection [3], allowing the study of body parts or areas that are not routinely dissected during a standard autopsy, such as the viscerocranium, cranio-cervical junction, larynx, shoulder girdle, pelvis, extremities and soft tissue of the back [4-7]. Furthermore, while the traditional autopsy determines a destruction of the residual findings, PMCT allows preserving images for re-evaluation and reinterpretation over time, also with the aid of post-processing 3D reconstructions. PMCT represents a useful procedure in many forensic scenarios that are often very difficult to interpret only with conventional autopsy [8-12], as in the case of decomposed bodies, because putrefaction processes can impressively alter the appearance of corps and consequently add more difficulty in determining the cause of death. In fact, body decomposition is determined by a combination of fermentation processes by gastrointestinal flora, aggression of external bacteria and other micro-organisms, and autolytic digestion of body tissues by endogenous enzymes. The rate and extent of post-mortem changes and decomposition processes are quite variable and are dependent on the cause of death and the external environment [13]. As a consequence, examination of a putrefied body represents a remarkable challenge for the forensic pathologists [14, 15].

Gas formation is a hallmark feature of putrefaction, since gaseous bloating in advanced decomposed bodies is determined by vascular and intra-parenchymatous gases. PMCT allows to detect exact localization of post-mortem gas in the whole body, even in very small amounts, and to distinguish between normal decomposition processes and pathologic gas collections that may have contributed to causing the death, such as air embolism, pneumothorax or pneumoperitoneum [16-27].

The aim of the present study is to report radiological findings and features in advanced decomposed bodies obtained by PMCT, even if possible with autopsy correlation. An overview of the radiological cadaveric modifications in different anatomical sites, due to natural decomposition processes that can be mistaken for pathologic processes, is also offered.

Materials and methods

Subjects

This retrospective descriptive multicentric study was conducted between May 2013 and November 2016, including forensic cases selected among those admitted to the medicolegal centres of Rome, Foggia, and Ferrara (Italy) by the local inquiring authorities to ascertain the cause of death. 41 cases (29 males, 12 females) were included for this study, selecting exclusively bodies with putrefactive signs at the external examination. 11 bodies (cases 1-11) were exhumed on the order of a judge, while 30 bodies (cases 12-41) were found at the crime scenes (**Table 1**). The post-mortem interval (PMI) ranged from 4 to 930 days (mean 194.9 ± 296.3 SD). Cases 1-11 consisted of subjects deceased in a hospital with an ascertained PMI as obtained from clinical records, while cases 12-41 were found dead after a presumptive PMI (± SD), reconstructed on the base of testimonies and forensic considerations. The age ranged from 18 to 90 years (mean 50.5 ± 21.8 SD).

PMCT acquisition

All the bodies were PMCT-scanned prior to autopsy. PMCT-scans were performed on a 64-section CT system (Somatom® Sensation Cardiac 64-slice scanner; Siemens, Forchheim, Germany) according to standardized scanning protocol: tube voltage 120 kV; tube current 250 mAs; section thickness 0.6 mm; reconstruction interval 0.5 mm; gantry rotation time 0.5-second; pitch 0.9. The bodies were wrapped inside an artifact-free body bag; all subjects were scanned in the supine position. All PMCT-scans were performed without administration of contrast agents. PMCT-data were transferred to a workstation for post-processing images reconstruction, performed with a slice thickness of 1.25 mm in increments of 0.7 mm, using soft tissue deconvolution algorithm (B20 kernel) and bone-weighted deconvolution filter (B46 kernel). Images were finally analysed using a viewing software (OsiriX® v.5.8.2 32-bit; Pixmeo, Geneva, Switzerland), calculating two-dimensional sagittal and coronal reformations and volume rendering (VR) reconstructions.

The present study was conducted in accordance with the Helsinki Declaration. As all the exams were parts of a complete forensic examination ordered by the local inquiring authorities, no specific consensus by the relatives was necessary prior to the realization of all PMCT; after the exam, all results were analysed anonymously. The processing of the data reported is covered by the general authorization to process personal data for scientific research purposes granted by the Italian Data Protection Authority (1 March 2012 as published in Italy's Official Journal no. 72 dated 26 March 2012) since the data do not entail any significant personalized impact on data subjects.

Image analysis

Images viewing and assessment was performed by 2 radiologists with expertise in forensic radiology (2 and 30 years of experience respectively) and 2 forensic pathologists trained in forensic imaging (3 and 35 years of experience respectively). To promote consistent assessments, a concordance was preliminarily tested between the investigators.

The internal putrefactive state was determined by the aforementioned observers using the radiological alteration index (RAI). RAI was determined by PMCT in 7 selected sites, including the major vessels (left innominate vena and abdominal aorta), selected bones (vertebra L3), selected organs (heart cavities, liver parenchyma and vessels, and kidney parenchyma) and subcutaneous tissues and muscles (subcutaneous pectoral tissues), according the standardized protocol by Egger et al. [28]. In particular, the grade of gas presence (0, I, II or III) was determined for the major vessels and selected bones (one gas bubble to completely filled with gas), and for the selected organs, subcutaneous tissues and muscles (one gas bubble to extensive emphysema). Once a grade was assigned for each site, according to the corresponding scores, the RAI was calculated.

Conventional autopsy

After PMCT-scans, the complete conventional autopsy of each body (examination of the cranial, thoracic and abdominal cavities) was performed by forensic pathologists.

The grade of external putrefaction (GEP) was assigned by the forensic pathologist during the external examination of the bodies, according to the standardized classification of Maujean et al. [29], based on the putrefaction signs described in the forensic literature:

- GEP1 ("beginning"): green skin discoloration was present in the abdomen area;
- GEP2 ("moderate"): detachment of the skin and/or blisters containing reddish

purplish serous liquid occurred at the extremities and in the sloping regions;

- GEP3 ("advanced"): putrefactive gases produced body swelling, eyes, and tongue protrusion and body fluids expulsion;
- GEP4 ("major"): fat liquefaction and/or darkening colouring of the integument and drying of the body extremities was observed;
- GEP5 ("mummified"): drying of the whole body with leather-like skin was evident.

A complete autopsy report was provided in all the cases, and causes of death were subsequently investigated by histological and toxicological examinations. Data obtained were secondarily compared to image analysis, in order to verify post-mortem radiological reports.

Statistical methods

A correlation between continuous variables has been investigated by linear regression analysis using Pearson's r correlation coefficient, R^2 coefficient of determination and adjusted R^2. In particular, the correlation between GEP and PMI, and RAI and PMI has been studied; the correlation between GEP and RAI has also been investigated.

Results

The PMCT-images evaluation and the analysis of putrefactive internal state revealed that, in all the examined cases, gas grade was > II in correspondence of the major vessels (left innominate vena and abdominal aorta), heart cavities, liver parenchyma, vertebra L3 and subcutaneous pectoral tissues; in correspondence of the kidney the gas grade varied from I to III (**Table 2**).

In the selected 7 sites, the RAI index was >61 in all bodies (interval 61-100, median 85) **(Table 3)**. In particular, in 7 (17%) cases RAI = 61 (grade II in all the selected sites), in 2 (5%) cases RAI = 70 (grade II in liver and vertebra L3, grade III in all the other sites), in 8 (19%) cases RAI = 78 (grade I in kidney, grade III in heart cavities and liver, grade II in the other sites), in 7 (17%) cases RAI = 85 (grade II in liver or vertebra L3, grade III in all the other sites), in 2 (5%) cases RAI = 93 (grade I in kidney, grade III in all the other sites) and in 15 (37%) cases RAI = 100 (grade III in all the selected sites) was determined.

Brain and nervous system

Cranial cavity was occupied almost entirely from gases. In particular, intracranial gas accumulation was observed in all cases, distributed on the top of the calvarium and in the vascular structures of the posterior cranial fossa; in 22/41 (54%) cases gas accumulation filled more than 50% of the whole intracranial space. Small gaseous collections were ubiquitously distributed within the brain parenchyma, with a "swiss-cheese" aspect; brain volume was reduced in all cases, placed in the sloping region of the calvarium. In all cases loss of definition of the grey-white matter junction and effacement of the sulci and ventricles were detectable. In 29/41 (71%) cases it was possible to recognize fully or partially the brainstem structures. Gas bubbles in the spinal canal were found in all cases examined (**Figure 1**).

Cardiovascular system

Intracavitary cardiac gas accumulation was detected in all the examined bodies and determined a relative dilatation of atria and ventricles; gas collections were observed also within the myocardium. Major vessels were collapsed and gas was symmetrically distributed throughout the vascular structure of the whole body (**Figure 2-3**).

Body cavities, soft tissues, and parenchymas

Putrefactive gas filled the thoracic and abdominal cavities. As a consequence of the degenerative processes, adipose degeneration and fat liquefaction associated with multiple gaseous collections were observed in all examined bodies, with a marked fluid collection in the pleural and peritoneal space. Soft and connective tissue were collapsed and showed gaseous degeneration, notably in correspondence of periskeletal muscular structures or in elective areas, i.e. gaseous ballooning of the scrotum. Parenchymatous organs were not completely recognizable in shape and appearance, liquefied and characterized by the collapse of the residual parenchymas. Lungs, liver, spleen, and kidneys appeared collapsed and reduced in size, homogenized to surrounding tissues (**Figure 4**).

Foreign bodies

Foreign bodies as pace-makers (3 cases), prosthetic mitral valves (1 case), orthopaedic prosthesis (4 hip and 3 knee) and surgical metallic clips were easily identified (**Figure 5-6**); renal and bladder stones were also recognized (**Figure 7)**.

Cadaveric external examination revealed in all cases the presence of transformative phenomena. Grade of external putrefaction (GEP) assigned in all the examined bodies resulted GEP3 (11/41, 27%) and GEP4 (18/41, 42%) in most of the cases, with body swelling, eyes and tongue protrusion, body fluids expulsion and fat liquefaction.

In particular, 2/41 (5%) bodies showed a parchmental consistency of the cutaneous similar to the old-leather; in all the other cases the skin showed a dark grey colour or, at most, yellowish with soft, elastic and rubbery consistency, similar to the recent-leather. Evident, more at the distal extremities of the limbs, large areas of post-mortal de-epithelialization. 5/41 (12%) bodies presented widespread phenomena of aggression by the fungal fauna, with numerous moulds, while all the exhumed bodies were soaked with cadaveric fluids.

At the cadaveric section, in all the examined bodies a widespread collapse of connective tissues and organs, which were much lesser recognizable in shape and appearance, was observed. In the cranial cavity, the dura mater resulted detached from the endocranium and the brain appeared of greyish pink colour, colliquated, homogenized and with polty consistency. In the thoracic cavity, the pleural space showed accumulation of serosanguinous putrefactive fluid or resulted covered with a mixture of brownish-blackish putrefactive liquid and fine yellowish granular residue; the lungs appeared collapsed towards the mediastinum, with pleura raised in bubbles, soft and pasty at palpation. The pericardial cavity contained serosanguinous putrefactive fluid or fine yellowish granular residue. The cardiac aspect was characterized by brown colour, flattened and empty, strongly reduced in form and consistency due to advanced putrefactive phenomena. The abdominal-peritoneal cavity contained an amount of putrefactive serosanguinous or yellowish liquid (decomposition transudates and/or liquefied fat). The intra-abdominal organs were reduced in volume, consistency, and size, pasty at palpation, due to advanced putrefactive phenomena. The vessels and perivasal tissues acquired a winey purplish hue, although liver and stomach resulted in dark brownish green. Distension of the bowel, with areas of patchy discoloration, was observed (**Figure 8**).

Autoptic findings were investigated, identified and described, and resulted consistent in all cases with the pathological radiological findings and the cause of death. In particular, in all the cases it was possible to determine a post-mortem diagnosis on the base of the radiological findings, confirmed by the autoptic data and histological-toxicological examinations.

Statistical analysis indicated a direct correlation between GEP-PMI (r 0.566; R^2 0,320; adjusted R^2 0.303; p <0.0001) and RAI-PMI values (r 0.472; R^2 0.223; adjusted R^2 0.203; p <0.001), with a positive correlation. An important positive correlation has been established between the external and internal putrefactive phenomena by GEP-RAI values (r 0.816; R^2 0.666; adjusted R^2 0.658; p <0.0001).

Discussion

Our study offers an overview of the common findings in advanced decomposition processes, that may dramatically alter the body's appearance and consequently add more difficulty in determining the cause of death [3, 4]. In fact, the putrefactive processes are associated with the disappearance of body fluids and to a significantly increased risk of bias. Furthermore, in advanced putrefaction, the texture can be completely dissolved, leading to liquefaction of entire organs, as shown in the images analysis carried out in the present study [7, 14, 17]. These alterations often lead to misinterpretation of the radiological findings and to difficulties in the determination of cause and manner of death.

The knowledge of the standard PMCT findings following the post-mortem changes and the decomposition status is important when interpreting PMCT-images, because decomposition has a great impact on the imaging features. The aetiology of post-mortem gas detected on PMCT, in fact, can be multifactorial and not necessarily related to putrefaction [4, 7, 11, 14-19].

Decomposition gas normally occurs within 24-48-hour post-mortem and is typically produced by intestinal flora [18]. Gas can be also detected in many other conditions as sepsis, ischemia and tissue damage, which is associated with rapid decomposition and putrefaction [30]. Intravascular gas could also be produced during cardiopulmonary resuscitation (CPR): chest compression causes the vaporization of dissolved gas in blood and the rupture of pulmonary vessels, allowing the air to enter the pulmonary vein and reach the systemic circulation. Furthermore, in hospitalized subjects, the bronchovenous fistulas caused by endotracheal intubation and the alveolar rupture caused by positive-pressure ventilation barotrauma, may lead to intravascular gas entry [31-33].

On the other hand, putrefactive gas should not be mistaken for pathologic gas collections that may have contributed or caused the death, such as air embolism, pneumothorax, or pneumoperitoneum [20-24].

In all the above mentioned cases, asymmetric or focal gas collections should be considered suspicious and related to pathological or traumatic causes. These findings could be useful in order to differentiate between body changes related to putrefaction and those related to other causes, mainly violent death and pathologic processes. In our study an asymmetric soft tissue gas distribution was detected in perforating gunshot wounds through the chest in 2 cases, but these findings were clearly related to the underlying traumatic injury. In fact, gas presence was reported in many cases of penetrating trauma with associated lacero-contusive foci and air bubble at the entry site [17, 34].

Radiological imaging by PMCT, as an adjunct to conventional autopsy in advanced decomposed bodies, has been proven to be a useful tool in detecting post-mortem gas localization, even in very small amounts. Based on our experience to date, putrefactive gas appeared symmetrically distributed in the 41 examined bodies. In all the examined cases a symmetrical ubiquitous gas accumulation has been detected within the heart cavities, vascular system, body cavities, parenchymatous organs, soft tissues, and bones, as shown in Results.

Our results have demonstrated in all cases ubiquitously moderate-diffuse presence of gas (grade II to III), particularly in correspondence of soft subcutaneous tissues, vertebral body L3 and cardiovascular structures such as heart cavities, abdominal aorta and left innominate vein. Interestingly, parenchymatous organs have shown a different distribution pattern, as in correspondence of liver (grade II to III) and kidney (grade I to III) a different gaseous amount has been found. This partial exception could be explained by the fact that the perirenal capsule protects more the renal structure from the putrefactive phenomena, coinciding with the autoptic data confirming that kidney moderately resists putrefaction.

Furthermore, according to PMCT standardized imaging assessment and the subsequent statistical analysis conducted on GEP and RAI values, a strong positive correlation between the external and internal grade of putrefaction has been established. Therefore, from the present study, the combined use of GEP and RAI resulted useful in the assessment of the putrefactive state in advanced decomposed bodies, providing reliable data prior to autoptic investigation and supporting the forensic pathologist in the evaluation of cadaveric post-mortem changes [35].

Conclusion

According to this standardized approach, an objective description of the post-mortem transformative phenomena was offered. Assessment of external (GEP) and internal (RAI) grade of putrefaction is even more important, considering its decisive role as an aid in discriminating the various causes of death, particularly confused by the overlap of putrefactive phenomena. Furthermore, detection of pattern distribution of gas could represent an aid to better discriminate between putrefactive processes and potential causes of death.

Conclusively, a correct interpretation process of the PMCT-data in advanced decomposed bodies is essential to avoid images pitfalls, due to natural decomposition processes that can be mistaken for pathologic processes.

References

1. Lichtenstein JE (1996) Forensic radiology. In: Gagliardi RA, McClennan BL (eds.) A History of the Radiological Sciences Diagnosis, CRC Press, Boca Raton, pp 579-605.
2. Bolliger SA, Thali MJ (2015) Imaging and virtual autopsy: looking back and forward. Philos Trans R Soc Lond B Biol Sci 370(1674), pii: 20140253. doi: 10.1098/rstb.2014.0253.
3. Dirnhofer R, Jackowski C, Vock P, Potter K, Thali MJ (2006) VIRTOPSY: minimally invasive, imaging-guided virtual autopsy. Radiographics 26:1305-1333. doi: 10.1148/rg.265065001.
4. Lundström C, Persson A, Ross S, Ljung P, Lindholm S, Gyllensvärd F, Ynnerman A (2012) State-of-the-art of visualization in post-mortem imaging. APMIS 120:316-326. doi: 10.1111/j.1600-0463.2011.02857.x.
5. Krentz BV, Alamo L, Grimm J, Dédouit F, Bruguier C, Chevallier C, Egger C, Da Silva LFF, Grabherr S (2016) Performance of post-mortem CT compared to autopsy in children. Int J Legal Med 130:1089-1099. doi: 10.1007/s00414-016-1370-z.
6. Grabherr S, Grimm JM, Heinemann A (2016) Atlas of Postmortem Angiography. Springer International Publishing, London.
7. Ishida M, Gonoi W, Okuma H, Shirota G, Shintani Y, Abe H, Takazawa Y, Fukayama M, Ohtomo K (2015) Common Postmortem Computed Tomography Findings Following Atraumatic Death: Differentiation between Normal Postmortem Changes and Pathologic Lesions. Korean J Radiol 16:798-809. doi: 10.3348/kjr.2015.16.4.798.
8. Silva RF, Botelho TL, Prado FB, Kawagushi JT, Daruge Júnior E, Bérzin F (2011) Human identification based on cranial computed tomography scan: a case report. Dentomaxillofac Radiol 40:257-61. doi: 10.1259/dmfr/96080236.
9. Busardò FP, Frati P, Santurro A, Zaami S, Fineschi V (2015) Errors and malpractice lawsuits in radiology: what the radiologist needs to know. Radiol Med 120:779-784. doi: 10.1007/s11547-015-0561-x.
10. Grabherr S, Heinemann A, Vogel H, Rutty G, Morgan B, Woźniak K, Dedouit F, Fischer F, Lochner S, Wittig H, Guglielmi G, Eplinius F, Michaud K, Palmiere C, Chevallier C, Mangin P, Grimm JM (2018) Postmortem CT Angiography Compared with Autopsy: A Forensic Multicenter Study. Radiology 288:270-276.

doi: 10.1148/radiol.2018170559.

11. Coty JB, Nedelcu C, Yahya S, Dupont V, Rougé-Maillart C, Verschoore M, Ridereau Zins C, Aubé C (2018) Burned bodies: post-mortem computed tomography, an essential tool for modern forensic medicine. Insights Imaging 9:731-743. doi: 10.1007/s13244-018-0633-2.
12. Le Blanc-Louvry I, Thureau S, Duval C, Papin-Lefebvre F, Thiebot J, Dacher JN, Gricourt C, Touré E, Proust B (2013) Post-mortem computed tomography compared to forensic autopsy findings: a French experience. Eur Radiol 23:1829-35. doi: 10.1007/s00330-013-2779-0.
13. Pinheiro J (2006) Decay Process of a Cadaver. In: Schmitt A, Cunha E, Pinheiro J (eds.) Forensic Anthropology and Medicine. Complementary Sciences from Recovery to Cause of Death. Humana Press Inc, Totowa, pp 85-116.
14. Zech WD, Jackowski C, Buetikofer Y, Kara L (2014) Characterization and differentiation of body fluids, putrefaction fluid, and blood using Hounsfield unit in postmortem CT. Int J Legal Med 128:795-802. doi: 10.1007/s00414-014-1030-0.
15. Byard RW, Tsokos M (2013) The challenges presented by decomposition. Forensic Sci Med Pathol 9:135-137. doi: 10.1007/s12024-012-9386-2.
16. Tschui J, Jackowski C, Schwendener N, Schyma C, Zech WD (2016) Post-mortem CT and MR brain imaging of putrefied corpses. Int J Legal Med 130:1061-1068. doi: 10.1007/s00414-016-1385-5.
17. Levy AD, Harcke HT, Mallak CT (2010) Postmortem Imaging: MDCT Features of Postmortem change and decomposition. Am J Forensic Med Pathol 31:12–17. doi: 10.1097/PAF.0b013e3181c65e1a.
18. Singh MK, O'Donnell C, Woodford NW (2009) Progressive gas formation in a deceased person during mortuary storage demonstrated on computed tomography. Forensic Sci Med Pathol 5:236-242. doi: 10.1007/s12024-009-9103-y.
19. Thali MJ, Yen K, Schweitzer W, Vock P, Ozdoba C, Dirnhofer R (2003) Into the decomposed body-forensic digital autopsy using multislice-computed tomography. Forensic Sci Int 134:109-114.
20. Egger C, Bize P, Vaucher P, Mosimann P, Schneider B, Dominguez A, Meuli R, Mangin P, Grabherr S (2012) Distribution of artifactual gas on post-mortem multidetector computed tomography (MDCT). Int J Legal Med 126:3-12. doi: 10.1007/s00414-010-0542-5.

21. Gebhart FT, Brogdon BG, Zech WD, Thali MJ, Germerott T (2012) Gas at postmortem computed tomography – An evaluation of 73 non-putrefied trauma and non-trauma cases. Forensic Sci Int 222:162-169. doi: 10.1016/j.forsciint.2012.05.020.
22. Ishida M, Gonoi W, Hagiwara K, Takazawa Y, Akahane M, Fukayama M, Ohtomo K (2011) Intravascular gas distribution in the upper abdomen of non-traumatic in-hospital death cases on postmortem computed tomography. Leg Med 13:174-179. doi: 10.1016/j.legalmed.2011.03.002.
23. Varlet V, Smith F, Giuliani N, Egger C, Rinaldi A, Dominguez A, Chevallier C, Bruguier C, Augsburger M, Mangin P, Grabherr S (2015) When gas analysis assists with postmortem imaging to diagnose causes of death. Forensic Sci Int 251:1-10. doi: 10.1016/j.forsciint.2015.03.010.
24. Morgan B, Adlam D, Robinson C, Pakkal M, Rutty GN (2014) Adult post-mortem imaging in traumatic and cardiorespiratory death and its relation to clinical radiological imaging. Br J Radiol 87:20130662. doi: 10.1259/bjr.20130662.
25. Offiah CE, Dean J (2016) Post-mortem CT and MRI: appropriate post-mortem imaging appearances and changes related to cardiopulmonary resuscitation. Br J Radiol 89:20150851. doi: 10.1259/bjr.20150851.
26. Charlier P, Carlier R, Roffi F, Ezra J, Chaillot PF, Duchat F, Huynh-Charlier I, Lorin de la Grandmaison G (2012) Postmortem abdominal CT: assessing normal cadaveric modifications and pathological processes. Eur J Radiol 81:639-647. doi: 10.1016/j.ejrad.2011.01.054.
27. Wagensveld IM, Blokker BM, Wielopolski PA, Renken NS, Krestin GP, Hunink MG, Oosterhuis JW, Weustink AC (2017) Total-body CT and MR features of postmortem change in in-hospital deaths. PLoS One 12:e0185115. doi: 10.1371/journal.pone.0185115.
28. Egger C, Vaucher P, Doenz F, Palmiere C, Mangin P, Grabherr S (2012) Development and validation of a postmortem radiological alteration index: the RA-Index. Int J Legal Med 126:559-566. doi: 10.1007/s00414-012-0686-6.
29. Maujean G, Vacher P, Bagur J, Guinet T, Malicier D (2016) Forensic Autopsy of Human Decomposed Bodies as a Valuable Tool for Prevention: A French Regional Study. Am J Forensic Med Pathol 37:270-274. doi: 10.1097/PAF.0000000000000266.
30. Sakata M, Miki A, Kazama H, Morita M, Yasoshima S (1980) Studies on the

composition of gases in the post-mortem body: animal experiments and two autopsy cases. Forensic Sci Int 15:19-29.

31. Hwang SL, Lieu AS, Lin CL, Liu GC, Howng SL, Kuo TH (2005) Massive cerebral air embolism after cardiopulmonary resuscitation. J Clin Neurosci 12:468-469.
32. Shiotani S, Ueno Y, Atake S, Kohno M, Suzuki M, Kikuchi K, Hayakawa H (2010) Nontraumatic postmortem computed tomographic demonstration of cerebral gas embolism following cardiopulmonary resuscitation. Jpn J Radiol 28:1-7. doi: 10.1007/s11604-009-0372-x.
33. Shiotani S, Kohno M, Ohashi N, Atake S, Yamazaki K, Nakayama H (2005) Cardiovascular gas on non-traumatic postmortem computed tomography (PMCT): the influence of cardiopulmonary resuscitation. Radiat Med 23:225-229.
34. Wilson AJ. Gunshot injuries: what does a radiologist need to know? Radiographics 19:1358-68.
35. Pomara C, Fineschi V, Scalzo G, Guglielmi G (2009) Virtopsy versus digital autopsy: virtual autopsy. Radiol Med 114:1367-1382. doi: 10.1007/s11547-009-0435-1.

Table 1. Description of the main characteristics of 41 advanced decomposed bodies including sex, age, cause of death and post-mortem interval (PMI)

Cases	Sex	Age (years)	Cause of death	PMI (days)
1	M	73	Haemorrhagic shock after femur fracture	428
2	M	90	Cardiogenic syncope	686
3	M	88	Hearth failure by bleeding and anaemia	887
4	F	88	Acute bleeding in chronic subdural hematoma	735
5	M	82	Hearth failure by anaemia	633
6	M	85	Haemorrhagic shock after femur fracture	740
7	F	77	Bleeding in non-Hodgkin's lymphoma	694
8	M	73	Haemorrhagic shock	521
9	M	59	Cardiogenic pulmonary oedema	930
10	F	77	Multi-organ failure	180
11	M	45	Septic shock	40
12	M	84	Ischemic cardiomyopathy	634 ± 89
13	M	53	Hearth failure in alcohol intoxication	7 ± 1
14	M	50	Traumatic brain injury	5 ± 1
15	F	43	Fatal firearm injury	90 ± 5
16	F	36	Fatal firearm injury	4 ± 1
17	F	47	Asphyxia	14 ± 5
18	M	50	Hearth failure	33 ± 1
19	M	27	Fatal firearm injury	120 ± 10
20	M	48	Hearth failure in chronic alcohol abuse	30 ± 5
21	M	31	Hearth failure	5 ± 1
22	M	29	Arrhythmia in cocaine abuse	4 ± 1
23	F	49	Dismemberment after fatal strangling	4 ± 1
24	M	19	Accidental train falling injury	4 ± 1
25	F	30	Drowning	180 ± 90
26	M	41	Fatal firearm injury	30 ± 5
27	M	24	Traumatic brain injury	4 ± 1
28	M	49	Cardiogenic pulmonary oedema	12 ± 2
29	F	84	Cardiogenic pulmonary oedema	6 ± 1
30	F	47	Asphyxia	12 ± 2
31	M	40	Drowning	25 ± 5
32	M	50	Drowning	25 ± 5
33	M	55	Drowning	150 ± 30
34	M	23	Drowning	15 ± 5
35	M	42	Drowning	13 ± 2
36	F	36	Asphyxia	13 ± 2
37	F	24	Slaughtering	35 ± 5
38	M	39	Cardiogenic pulmonary oedema	7 ± 1
39	M	18	Hanging	6 ± 1
40	M	34	Frostbite	25 ± 5
41	M	30	Cardiogenic pulmonary oedema	4 ± 1

PMI: Post-Mortem Interval. Cases 1-11: ascertained PMI as obtained from clinical records; cases 12-41: presumptive PMI (± SD) reconstructed on the base of testimonies and forensic considerations

Table 2. Gas grade and score determined for 7 selected sites

Sites	Gas grades	Scores	Number of cases
Heart cavities	I	1	N = 0
	II	8	N = 7
	III	17	N = 34
Liver parenchyma and vessels	I	1	N = 0
	II	5	N = 13
	III	20	N = 28
Left innominate vena	I	5	N = 0
	II	15	N = 15
	III	15	N = 26
Abdominal aorta	I	8	N = 0
	II	8	N = 15
	III	8	N = 26
Kidney parenchyma	I	0	N = 8
	II	7	N = 7
	III	7	N = 26
Vertebra L3	I	5	N = 0
	II	10	N = 20
	III	25	N = 21
Subcutaneous pectoral tissues	I	8	N = 0
	II	8	N = 15
	III	8	N = 26

Table 3. Grade of external putrefaction (GEP) assessment and radiological alteration index (RAI)

Case no.	GEP	RAI	Cases	GEP	RAI
1	5	85	**21**	2	61
2	4	100	**22**	2	61
3	4	100	**23**	2	78
4	4	78	**24**	1	61
5	4	100	**25**	4	100
6	4	100	**26**	3	85
7	4	100	**27**	1	61
8	4	93	**28**	3	78
9	4	100	**29**	2	78
10	4	100	**30**	3	78
11	3	93	**31**	4	100
12	5	85	**32**	4	100
13	3	85	**33**	4	100
14	2	61	**34**	4	100
15	4	100	**35**	4	100
16	1	61	**36**	3	78
17	3	78	**37**	4	85
18	3	85	**38**	3	70
19	4	100	**39**	3	70
20	3	85	**40**	2	78
			41	2	61

GEP (Grade of External Putrefaction) was assessed from GEP1 (beginning) to GEP5 (mummified). RAI (Radiological Alteration Index) was determined from 61 to 100 (min 0 - max 100)

Figures legend

Figure 1. Axial PMCT images demonstrate intracranial gas accumulation distributed on the top of the calvarium and inside the vascular structures; brain parenchyma results liquefied, with loss of definition of the grey-white matter junction and effacement of the sulci and ventricles (Case N. 3, M 88yo, PMI 887 days, cause of death: hearth failure by bleeding and anaemia, GEP 4, RAI 100).

Figure 2. Axial PMCT thoracic section demonstrate gas accumulation with symmetrical distribution in the heart cavities and in vascular system (Case N. 6, M 85yo, PMI 740 days, cause of death: haemorrhagic shock after femur fracture, GEP 4, RAI 100).

Figure 3. Coronal reconstruction showing gas accumulation in cardiovascular system and gaseous degeneration of all parenchymal abdominal organs and soft tissues (Case N. 1, M 73yo, PMI 428 days, cause of death: haemorrhagic shock after femur fracture, GEP 5, RAI 85).

Figure 4. Axial PMCT demonstrate putrefactive gas filling chest and abdominal cavities with involvement of liver parenchyma, hepatic veins, soft and connective tissues (Case N. 2, M 90yo, PMI 686 days, cause of death: cardiogenic syncope, GEP 4, RAI 100).

Figure 5. PMCT image on axial plane demonstrate presence of prosthetic mitral valve; heart cavities and vessels are filled with gas (Case N. 8, M 73yo, PMI 521 days, cause of death: haemorrhagic shock, GEP 4, RAI 93).

Figure 6. 3D Volume rendering with bone tissue reconstruction filter helps to emphasize skeletal structures, pace-maker and external metallic object (Case N. 5, M 82yo, PMI 633 days, cause of death: hearth failure by anaemia, GEP 4, RAI 100).

Figure 7. PMCT image on axial plane shows a renal stone on the left kidney (Case N. 8, M 73yo, PMI 521 days, cause of death: haemorrhagic shock, GEP 4, RAI 93).

Figure 8. (A-D) Autopsy findings: dura mater detached from the endocranium (A);

brain colliquated, homogenized and with polty consistency (B); heart flattened and empty, strongly reduced in form and consistency (C); intra-abdominal putrefactive phenomena (D). (E-G) Histological evidence of putrefactive alteration of the heart (E), lung (F) and kidney (G).

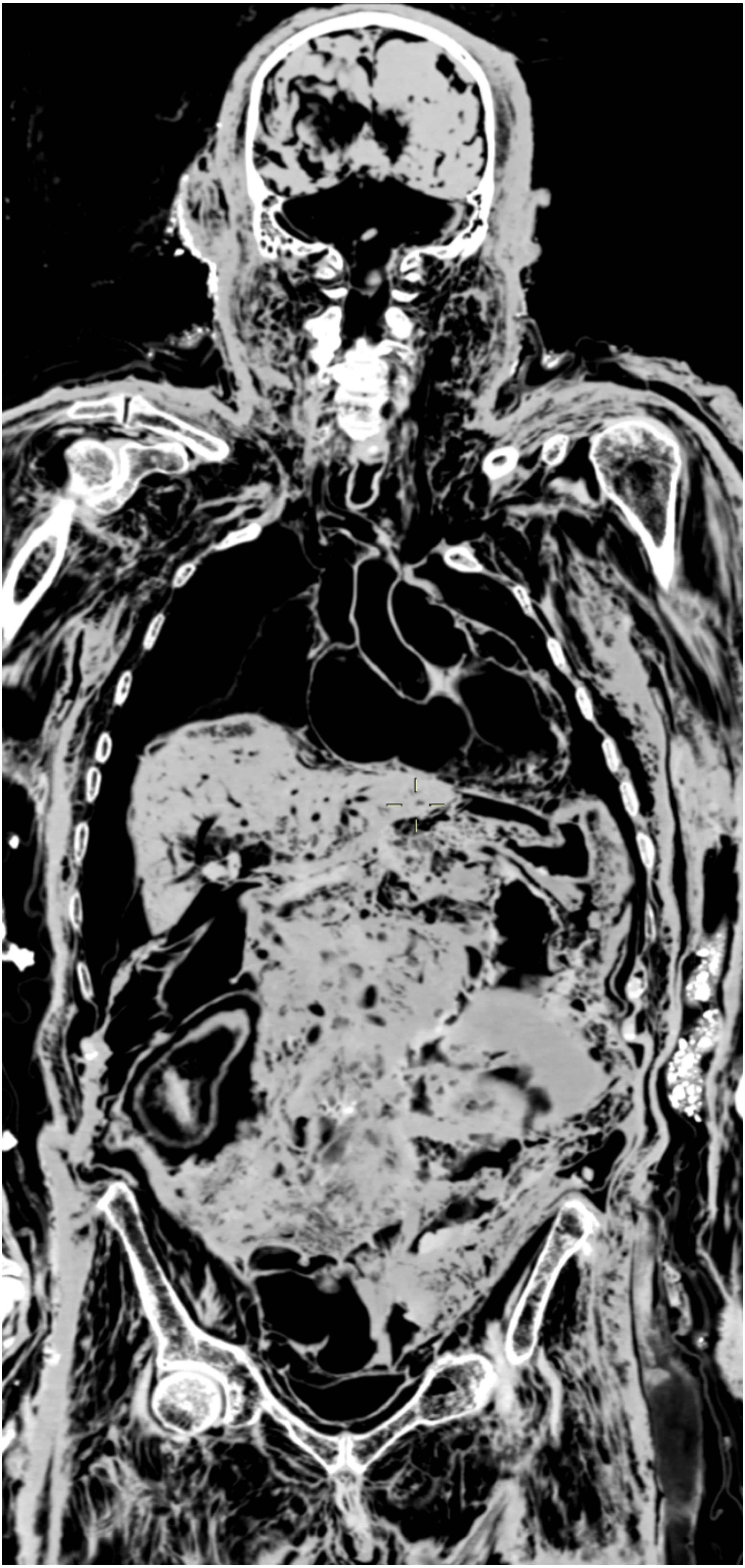

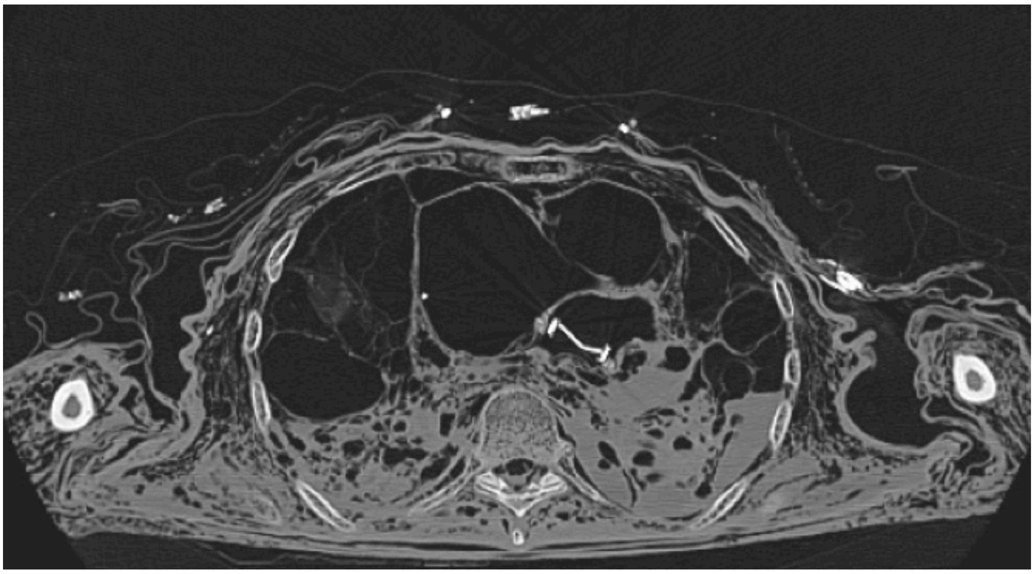


S

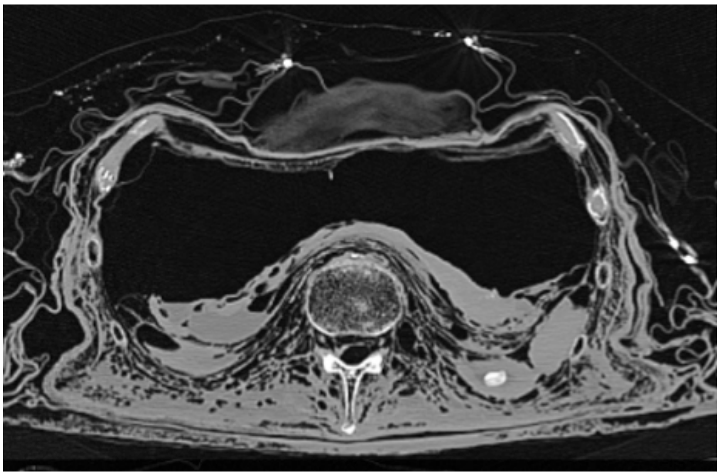

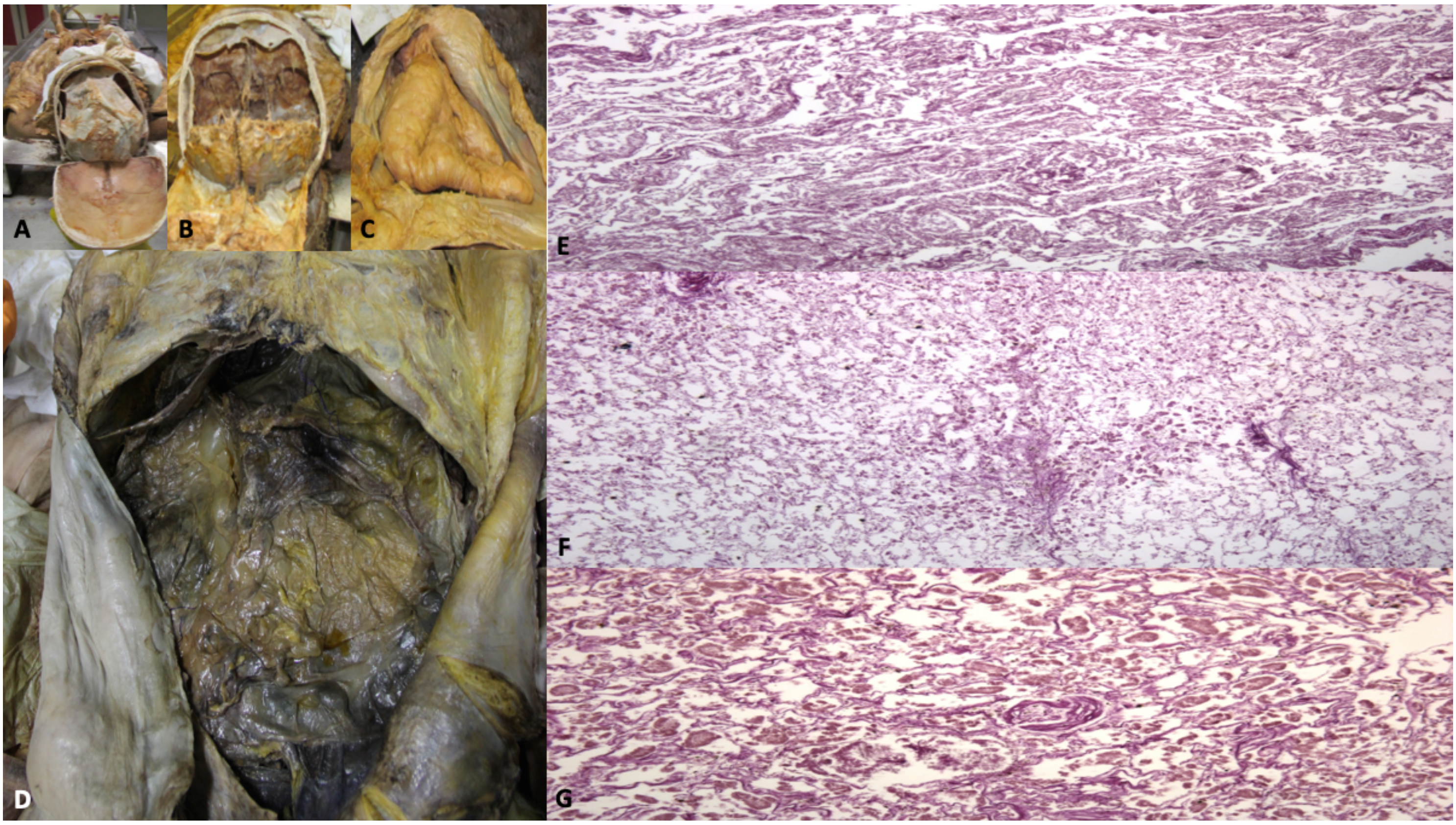
A
B
C
D
E
F
G